8 March 1999

PHYSICS LETTERS A

ELSEVIER

Physics Letters A 252 (1999) 297–306

Compactons in a class of nonlinearly quintic equations

Philip Rosenau [a,1], Doron Levy [b,2]

[a] *School of Mathematical Sciences, Tel-Aviv University, Tel-Aviv 69978, Israel*

[b] *Department of Mathematics, University of California, Berkeley, CA 94720, and Lawrence Berkeley National Lab, Berkeley, USA*

Received 12 August 1998; revised manuscript received 23 December 1998; accepted for publication 4 January 1999
Communicated by C.R. Doering

Abstract

We introduce a nonlinear dispersive quintic equation. Its travelling waves are governed by a linear equation. We construct a large variety of explicit compact solitary waves. Some of these compactons are very robust, others decompose very quickly. Numerical simulations also reveal the existence of compact travelling breathers. © 1999 Published by Elsevier Science B.V.

1. Introduction

In this work we extend our studies of the nonlinearly dispersive partial differential equation $K(m,n)$ [1–4],

$K(m,n)$;

$$u_t + (u^m)_x + (u^n)_{xxx} = 0\,, \quad n \geqslant 1\,, \tag{1}$$

to consider higher order dispersive effects. Among the novel feature of Eq. (1), we mention the non-analyticity of some of its more interesting solutions, or the compactness of solitary waves. For $n = m$ these solitary waves, the so-called *compactons*, take a particularly simple form,

$$u = \left\{ \frac{2n\lambda}{n+1} \cos\left[\frac{n-1}{4n}(x-\lambda t) \right] \right\}^{2/(n-1)} \quad \text{for } |x-\lambda t| \leqslant \frac{2n\pi}{n-1}\,, \tag{2}$$

and u vanishes elsewhere. The emergence of such structures is best seen via an explicit analysis of traveling waves [1,4]. It was demonstrated numerically that even though in general, for $n > 1$, Eq. (1) is not integrable, nevertheless the interaction between their compact structures is *very robust*, leaving very little debris behind and the interacting compactons persist for hundreds of interactions [1]. Integrable equations admitting compactons are discussed in Refs. [2,5]. In this paper we focus our attention on *fifth order nonlinear dispersion* and present a family of explicit, single and multi-hump, compact solitary solutions. Though

$$u_t + (u^m)_x + (u^m)_{3x} + \delta(u^m)_{5x} = 0 \tag{3}$$

can be considered as a natural quintic extension of Eq. (1), our starting point is

$$u_t + (u^{m+1})_x + [u(u^n)_{xx}]_x = 0\,. \tag{4}$$

Eq. (4), which is similar to Eq. (1), also admits compact structures which are very similar to those of (1). Its quintic extension will be seen to be amenable to analysis,

[1] E-mail: rosenau@math.tau.ac.il.
[2] E-mail: dlevy@math.berkeley.edu.

PII S0375-9601(99)00012-2

$Q(l,m,n)$;

$$u_t + a(u^{m+1})_x + \omega[u(u^n)_{xx}]_x + \delta[u(u^l)_{4x}]_x = 0\,. \tag{5}$$

Unless otherwise stated we shall assume that $a = \omega = 1$. To find traveling waves with a constant speed we define $s = x - \lambda t$ and integrate once to obtain

$$-\lambda u + u^{m+1} + u(u^n)_{ss} + \delta u(u^l)_{4s} = C_0 (= \text{const.}) \tag{6}$$

Disregarding the integration constant we cast Eq. (6) into the obvious product $u\mathbf{L}[u(s)]$. In particular, if $n = m = l$, we obtain a linear equation in $\mathbf{L}[V(s)]$ where $V = u^l$, and

$$\mathbf{L}[V(s)] \doteq -\lambda + V + V_{ss} + \delta V_{4s} = 0\,. \tag{7}$$

We thus obtain an unusual, yet very useful, situation wherein *the equation governing traveling waves is linear*. Superposition of solutions enables to generate a wide variety of patterns. Though these patterns may, or may not, be evolutionary, nevertheless, the linearity of the fourth order differential equation like (7) is an essential feature. In fact, almost any nonlinear element, when added, makes this equation unsolvable. Note that not much is lost when the integration constant C_0 is disregarded. Indeed, if u vanishes at the front and $l = 1$, the dominant part $uu_{4s} = C_0$ cannot be balanced unless $C_0 = 0$. For $l = 2$, however, such a balance is possible yielding $u \sim s^{4/3}$ near $u = 0$. These solutions are thus lost when C_0 is disregarded.

The present studies of the quintic equation are motivated in part by our quest to understand how far the concept of compact structures can be extended, but primarily *by our quest to find a quintic model which, even if only of a pedagogical value, would explain the richness of the structures generated by the variety of the quintic models.* In this respect one should keep in mind that for almost two decades quintic models have resisted almost all analytical attempts, and even the elementary quest to find a simple solitary wave cannot be answered in general, see Ref. [6,7], and references therein. Most of our present knowledge about the patterns generated by quintic, dispersive partial differential equations, originates from numerical experiments. In contradistinction, the linearity of Eq. (7) provides a plethora of explicit travelling solutions. It is also of interest to note that patterns generated by the $K(2,2)$ equation and Eq. (4) are almost identical. Therefore, these two nonlinear forms of dispersion are almost interchangeable. Similarly, in spite of the differences between the quintic dispersion terms in Eqs. (5) and (3), the emerging patterns are quite similar. Finally, we call the attention to the appendix where we present a number of partial differential equations which also admit a linear subclass of travelling solutions.

2. Travelling waves

The nature of the travelling solutions obtained via Eq. (7) is determined by the roots of the bi-quadratic equation $\delta r^4 + r^2 + 1 = 0$. Let

$$r^2 = -\Delta_\pm\,, \quad \Delta_\pm = [1 \pm \sqrt{1 - 4\delta}]/2\delta\,,$$

and consider first purely imaginary roots. We have

Case 1.

$$0 < \delta < 1/4 \Rightarrow r = \pm \mathrm{i}\sqrt{\Delta_\pm}\,.$$

In this case

$$V = \lambda + v_1 \cos[\sqrt{\Delta_-}(s + s_1)] + v_2 \cos[\sqrt{\Delta_+}(s + s_2)]\,, \tag{8}$$

with constants v_i and s_i, $i = 1, 2$. The basic compacton solution is obtained upon setting either of the integration constants to zero. We obtain

$$u^l \equiv V = 2\lambda \cos^2[\sqrt{\Delta_\pm}s/2] \quad \text{for } |s| \leqslant \pi/\sqrt{\Delta_\pm}\,, \tag{9}$$

and zero elsewhere. Since $\Delta_+ > \Delta_-$, we have a narrow, Δ_+ compacton, which later will be shown to be unstable, and Δ_-, a wide compacton, which later will be shown to be stable. Since Eq. (7) is linear and each of the solutions is invariant under shifts in s, a two parameter family of solutions may be constructed. To generate compactons, V has to vanish on the front at least as s^2, which implies that this point must be a local extremum of the solution. To see how such a construction is done, consider, for instance, the periodicity ratio, p, being equal two, i.e., $p := \sqrt{\Delta_+/\Delta_-} = 2$, which happens for $\Delta_- = 5/4$ (and thus $\delta = 0.16$).

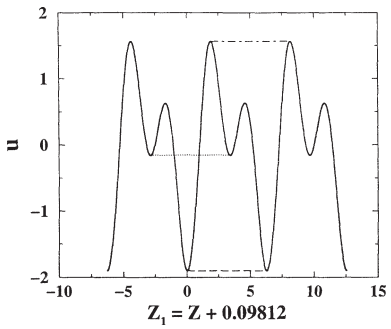

Fig. 1. An example of 2-periodic functions with three different 2-hump compactons that one can construct by properly shifting the elevation of V (note also a shift in Z to ensure that the double period coincides with the 0–2π interval).

Now let the homogeneous part of the solution be (see Fig. 1)

$$V_h = -\cos(z + 1/2) - \cos(2z), \quad z = \sqrt{5/4}s\,.$$

The choice of the shift $(1/2)$ is arbitrary and so is the fact that both periods have an equal weight in the solution. These are 2 degrees of freedom to choose from. In Fig. 1 we display three different possibilities to construct a 2-hump compacton. If for a given choice we get $V_h = V_0$ at the edge, then $V = \lambda[1 - V_h/V_0]$ vanishes smoothly at the edge of the domain.

Let us examine in more detail one particular class of solutions. Let the periodicity ratio $p = \sqrt{\Delta_+/\Delta_-}$ be an integer and the two waves in phase. Note that any periodicity ratio is possible with the corresponding δ given as

$$\delta = \left[\frac{p}{1+p^2}\right]^2. \tag{10}$$

Let $z = s\sqrt{\Delta_-}$ and consider a class of compact solutions,

$$V = \lambda[1 + (1 + (-1)^p b)\cos z + b\cos pz\,] \quad \text{for } |z| \leqslant \pi\,, \tag{11}$$

and zero elsewhere. The constant b is a free parameter. We thus have a one-parameter family of solutions.

As the first use of the free parameter we seek compact solutions with two smooth derivatives at the edge. The smoothness of the third derivative follows automatically. For $p = 2$ this yields $b = 1/3$ (for $p = 3$; $b = -1/8$, etc.) and the resulting solution reads

$$V = \frac{\lambda}{p^2-1}[p^2 - 1 + p^2\cos z + (-1)^p \cos pz\,] \quad \text{for } |z| \leqslant \pi\,, \tag{12}$$

and zero elsewhere. We shall refer to these solutions which have an extended smoothness at the edges as *P-compactons*. Their shape is markedly different for odd and even p's. For odd p's, the first three derivatives vanish at $z = 0$ as well, flattening the resulting pulse. For even p's the interaction between the two basic modes increases the amplitude but localizes the resulting compacton. These facts are evident when $p = 2$ and $p = 3$ cases are recorded explicitly,

$$p = 2\,; \quad V = \tfrac{8}{3}\lambda\cos^4(z/2) \quad \text{for } |z = s\sqrt{5}/2| \leqslant \pi \text{and} \quad \delta = 0.16\,, \tag{13}$$

$$p = 3\,; \quad V = 2\lambda[2 - \cos(z)]\cos^4(z/2) \quad \text{for } |z = s\sqrt{10}/3| \leqslant \pi \quad \text{and} \quad \delta = 0.09\,. \tag{14}$$

Let us follow the changes in the pattern (say, the number of humps) as b is varied. If

$$V'(z) = (1 + (-1)^p)b\sin z + pb\sin pz \neq 0 \quad \text{for } |z| \leqslant \pi\,,$$

only a simple, one hump, compacton is possible. For $p = 2$, this condition imposes $-1/5 \leqslant b \leqslant 1/3$. At the upper end of the domain, $b = 1/3$ and the 2-compacton solution (13) emerges. At the lower end, $b = -1/5$, we have a new compacton solution,

$$V = \frac{8\lambda}{5}[1 - \sin^4(z/2)] \quad \text{for } |z = \sqrt{5}s/2| \leqslant \pi\,, \tag{15}$$

with a flat top; $V' = V'' = V''' = 0$ at $z = 0$.

When b is moved out of the $[-1/5, 1/3]$ domain, the solution develops two humps. When $1/3 \leqslant b$ the extra smoothness at the edge is resolved into a negative well that emerges near the edge. Similarly, when b crosses the lower end of the domain, the extra smoothness at the center of the pulse resolves into an additional hump. The resulting solutions are always non-negative. These patterns are best seen taking two representative values of b,

For $b = 1$,

$$V = 4\lambda \cos(z)\cos^2(z/2)$$
$$\text{for } |z| \leqslant \pi,$$

For $b = -1/2$,

$$V = \lambda[3 - 2\cos(z)]\cos^2(z/2)$$
$$\text{for } |z| \leqslant \pi,$$

and zero elsewhere. These solutions were written in a way that shows how the basic compacton solution is modulated by the presence of the unstable Δ_+ component of the solution.

Consider now $p = 3$ ($z = s\sqrt{10}/3$, $\delta = 0.09$). One hump compactons reside in $-1/8 \leqslant b \leqslant 1/4$. At $b = -1/8$, a $P = 3$-compacton, given via (14), emerges. For $b < -1/8$ the solution develops three new humps; a negative hump near each edge and a positive hump near the center. At the upper limit, $b = 1/4$, we obtain a new compacton solution,

$$V = \lambda[1 + \cos^3(z)] \quad \text{for } |z| \leqslant \pi. \tag{16}$$

As $b = 1/4$ is crossed the inflection point at $|z| = \pi/2$ splits into two humps. The resulting multihump structure may be easily seen taking $b = 1/2$ (and any odd p),

$$V = \lambda\left\{1 + \tfrac{1}{2}[\cos(pz) + \cos(z)]\right\}$$
$$\text{for } |z| \leqslant \pi, \quad z = \sqrt{\Delta_-}\, s, \tag{17}$$

and zero elsewhere. In Section 3, we test the evolutionarity of these patterns for $p = 3$ and 5. When used as an initial data, instead of propagating in a constant speed, as expected from a travelling-wave, these solutions transform into stable *breathers* that propagate with a constant speed. In passing we also note the *stationary* compact solution

$$V(x) = V_0 \cos^3\left(\frac{\sqrt{10}}{3}\, x\right)$$
$$\text{for } |x| \leqslant 3\pi/2\sqrt{10}, \tag{18}$$

and zero elsewhere.

When p is a, non-integer, rational number m/n, one may form P-compactons but their width will be now n times the width of the elementary, Δ_-, compacton. We obtain

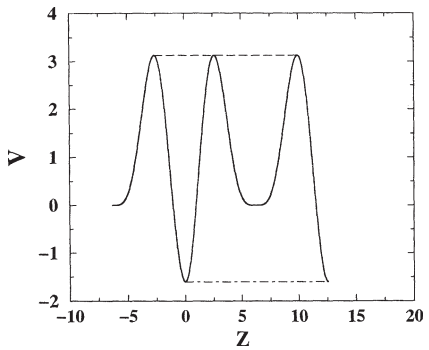

Fig. 2. An example of a a solution that for $|z| \leqslant 2\pi$ supports a 2-humps, P-Compacton, with $p = 3/2$. Note that a conventional, 2-hump, compacton is also possible if $0 \leqslant z \leqslant 4\pi$.

$$V = \lambda\left\{1 + \frac{1}{m^2 - n^2}\left[-m^2\frac{\cos z}{\cos(n\pi)} + n^2\frac{\cos(mz/n)}{\cos(m\pi)}\right]\right\} \quad \text{for } |z| \leqslant n\pi, \tag{19}$$

and zero elsewhere, see Fig. 2 for $p = 3/2$. Unlike the integer p case, wherein all P-compactons have only one hump, for $p = 3/2$ we have two humps. The figure also reveals a second, conventional, compacton with two humps and quite a flat bottom if $V \to V + 9/5$ and $0 \leqslant z \leqslant 4\pi$. In addition two, single hump, compactons are possible as well.

Case 2. For $\delta > 1/4$ we obtain complex Δ's. The resulting solution is then cast into

$$V(s) = \lambda + V_0 \cosh(\mu_+ s)\cos(\mu_- s), \tag{20}$$

or

$$V(s) = \lambda + V_0 \sinh(\mu_+ s)\sin(\mu_- s),$$

where V_0 is a constant and $\mu_\pm = [\sqrt{2 \pm 1/2\delta}]/2\delta^{1/4}$.

As before, for compact structures we request $V(s)$ to be smooth at the edge of the domain. Thus for (20) the two points at the edge have to be chosen from the nontrivial solutions of

$$K\tanh(Kz) = \tan(z),$$
$$K \equiv \frac{\mu_+}{\mu_-} = \sqrt{\frac{4\delta + 1}{4\delta - 1}}, \tag{21}$$

and $z = \mu_- s$. Eq. (21) has a countable number of solutions and each root enables a construction of a different compact solitary wave. Thus if s_i denotes

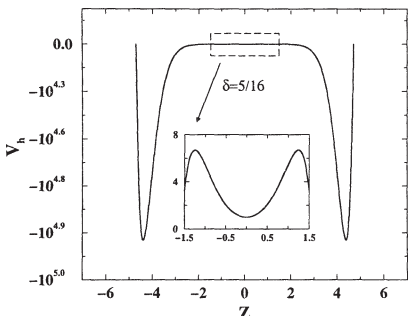

Fig. 3. A 2-humps travelling compacton for $\delta = 5/16$. The difference of scales, see the insert, causes this structure to look completely flat.

a solution of (21), then the corresponding compact solution is

$$V(s) = \lambda \left\{ 1 - \frac{\cosh(\mu_+ s)}{\cosh(\mu_+ s_i)} \frac{\cos(\mu_- s)}{\cos(\mu_- s_i)} \right\} \quad \text{for } |s| \leqslant s_i \,, \tag{22}$$

and vanishes elsewhere. Due to the very fast growth of the exponential factor it is nearly impossible to visualize the internal structure of these compactons. As can be seen from the example shown in Fig. 3 where $K = 3$ ($\delta = 5/16$), there is an enormous disparity of scales between the inner (see the insert) and the outer structure. For all practical purposes, this 2-humps compacton looks like a compacton with a flat plateau.

Case 3; $\delta < 0$. The solution may be written as

$$v = \lambda + v_1 \cosh(\Delta_h s) + v_2 \cos(\Delta_t s) \,, \tag{23}$$

or

$$v = \lambda + v_1 \cosh(\Delta_h s) + v_2 \sin(\Delta_t s) \,, \tag{24}$$

where

$$2|\delta|\Delta_h^2 = 1 + R \,, \quad 2|\delta|\Delta_t^2 = -1 + R, \quad R = \sqrt{1 + 4|\delta|} \,.$$

The first solution (23) generates symmetric compact structures. The second, Eq. (24), enables to construct a variety of asymmetric compact structures like the one shown in Fig. 4.

Case 4; $0 < \delta < 1/4$, *but* $\omega < 0$. In this case all roots of the indicial equation are real, and no travelling compact solution seems possible.

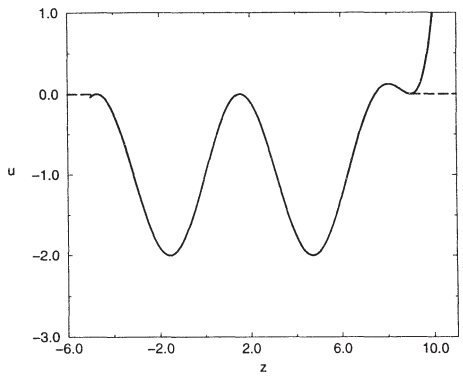

Fig. 4. Example of a compacton for $\delta < 0$.

3. Elements of numerical studies

The goal of this section is to sketch the basic time dependent features of our problem studied on a periodic domain, and to test the evolutionary aspects of the various solutions presented in the previous section. We describe a set of numerical experiments focusing our attention on the $l = m = n = 1$ case and the $0 < \delta < 1/4$ domain. A more detailed analysis and extensive numerical experiments are in progress.

3.1. Numerical issues

Though the $K(m, n)$, the first equation describing the propagation of compactons was introduced over half a decade ago, due to the strong nonlinearity and the non-analyticity of the solutions, the numerical issues concerning the numerical integration of this and other compacton-supporting equations are still considered to be far from being adequately understood.

At the present stage a full analysis of the convergence of the numerical scheme is a challenging task. We have only a partial understanding of the numerical methods used to study our problem. Practically, the only meaningful criterion to check the numerical convergence of our scheme is to monitor the behavior of the resulting solution as one refines the grid. The results obtained in all our simulations were found to be independent of the grid size. However, one still has to distinguish between genuine phenomena and those which are due to the numerics. This is of major importance, in particular due to the appearance of second-order interactions and oscillatory tails, which at this point cannot unambiguously be declared as a

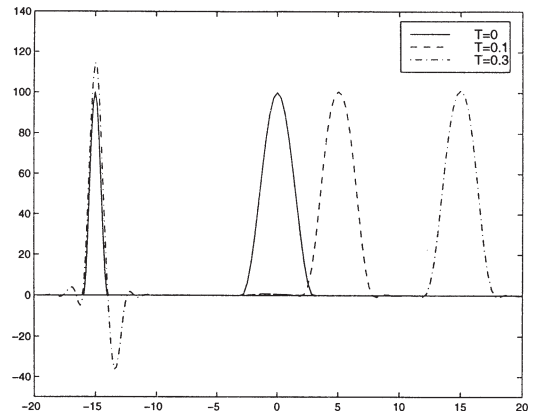

Fig. 5. A single compacton. Right: wide (Δ_-) stable. Left: narrow (Δ_+) unstable. $\delta = 0.09$.

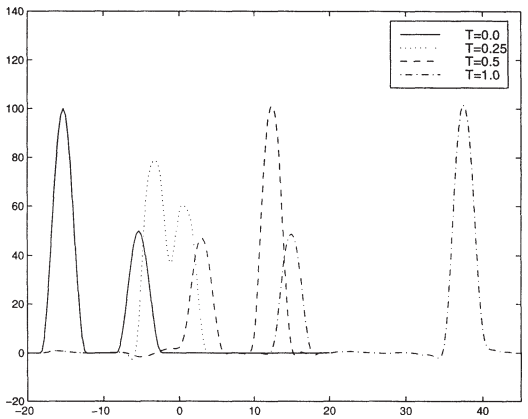

Fig. 6. Compacton–compacton interaction. $\delta = 0.09$.

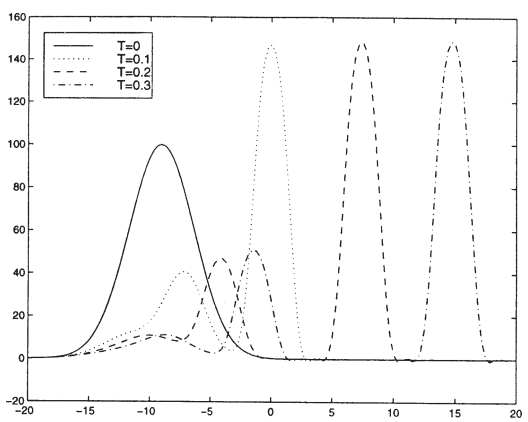

Fig. 7. $\delta = 0.09$. Gaussian initial data. It dissolves into $\cos^2$-shaped compactons

true effect or merely a numerical artifact.

The examples to be presented next are intended to display a flavor of the richness of the structures generated by our model. We find both stable and unstable structures. The unstable structures, typically associated with initial data that has both negative and positive parts, either transform into stable ones or develop oscillations that ultimately blowup in time.

3.2. Numerical simulations

In the following simulations we have used a pseudo-spectral method in space and explicit fourth-order Runge–Kutta method in time. Typically, we used 128 or 256 modes in the Fourier transform. The time step, Δt, was of the order of $(\Delta x)^5$, (Δx being the spatial grid size). In order to avoid the aliasing as well as to discard the numerical oscillations created by the nonsmooth front of the compacton, the solutions were filtered using a smooth exponential filter in the Fourier space, i.e., $e^{-\alpha(j/N)^p}$. Here, N is the total number of modes, j abbreviates the mode number, $\alpha = 34$, so that $e^{\alpha} \sim 10^{-16}$ (the roundoff error), and p depends on N. For $N = 128$ we used $p = 8$.

In Fig. 5 we test the evolutionarity of the basic single compacton (9). In the right part we follow the wider compacton, (Δ_-), while on the left the initial data corresponds to its narrow sibling, (Δ_+). In both cases, $\lambda = 50$. It is evident that the wider compacton is stable and propagates to the right, while the narrower one is unstable and radiates its energy.

In Fig. 6 we display the evolution and interaction of two stable compactons. They both emerge intact after the interaction, preserving their initial shape. Note the typical phase shift associated with solitonic interactions.

Fig. 7 demonstrates the emergence of stable compactons out of a more general initial data, which in this case is taken as $u(0) = 100\, e^{-0.07x^2}$, and $\delta = 0.09$. The emerging compactons are stable, and preserve their initial shape in subsequent interactions. One can easily verify that these compactons correspond to the wide branch of the $\cos^2$ solution, (9). A similar behavior was numerically observed for the same initial data and negative $\delta's$.

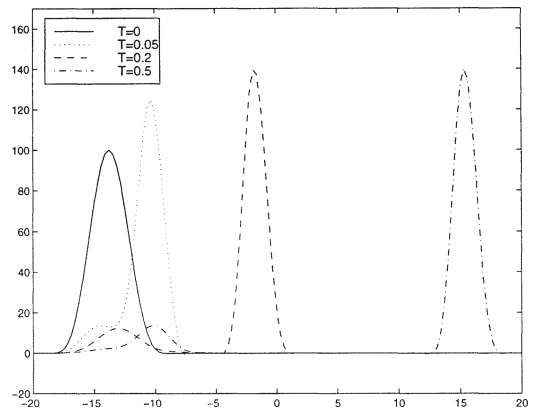

Fig. 8. $\delta = 0.16$. A relatively wide $\cos^4$-shaped initial data begets a tall $\cos^4$-compacton followed by a much smaller $\cos^2$-compacton.

3.2.1. P-compactons

The 2-compacton, (see (13)), was seen to be stable in our numerical simulations and has a meaningful domain of attraction. This is shown in Fig. 8 where we follow the evolution of the initial pulse $u(0) = 100\cos^4(\sqrt{0.1}x)$, with $\delta = 0.16$. The initial pulse has a wider support than the basic 2-compacton and thus decomposes into separate compactons. The leading, taller, compacton is a 2-compacton and has the $\cos^4$-shape, (13). The smaller compacton has the $\cos^2$ shape, (9). In this example we thus observe two stable canonical compactons emerge from a given initial datum. Actually the domain of attraction of the 2-compactons is much wider than can be inferred from the presented example. For instance, the compacton solutions corresponding to $b = -1/5$ (see (15)) and $b = -1/2$ decompose. The emerging pattern is quite similar to the pattern described in Fig. 8, and the leading pulse is, again, the 2-compacton!

We note that other single hump P-compactons also appear to be stable. For instance, the 4-compacton was observed to emerge from an initial datum having a similar shape but a wider support.

We now turn to more evolved patterns. First, consider Fig. 9 which displays the emergence of a 2-humps compact breather. Here the 3-humps travelling wave given in (17) for $\delta = 0.09$, was used as an initial datum. Clearly, this pattern rather than to propagate with a constant speed, decomposes into two parts – the left part is the narrow, unstable compacton, while the emerging right part is a *2-humps compact*

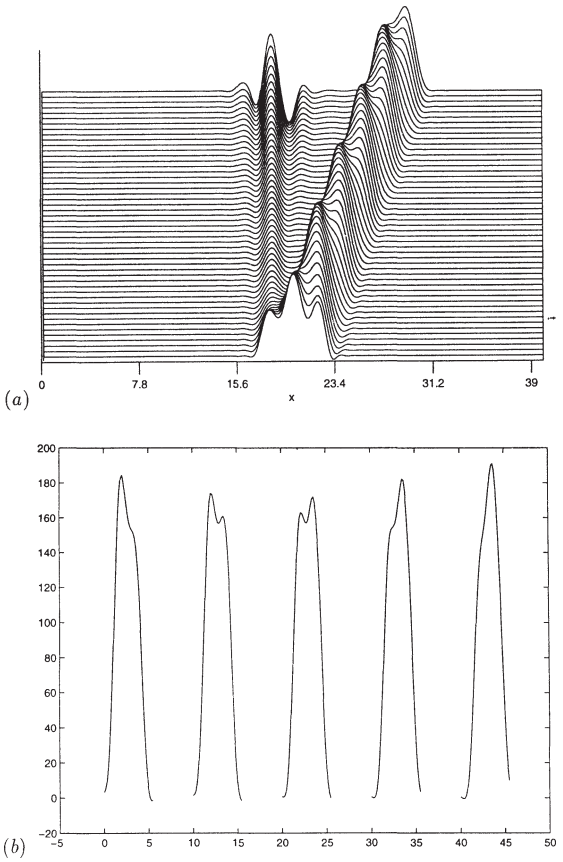

Fig. 9. (a) $\delta = 0.09$. A 3-humps travelling compacton, see (17), is used as an input. Though it is an exact solution, instead of shape preserving propagation it transforms into an unstable compacton, seen on the left, and a 2-humps breather. (b) A separate snap-shot of the breather in later times.

breather. The breather appears to be a stable structure that moves to the right with a constant speed and, as can be clearly seen, apart of having compact support, it has the typical features of a conventional breather. In Fig. 9a we show the temporal evolution of the solution for $t \in [0, 0.093]$. The time difference between every two frames equals $\Delta t = 1.865 \times 10^{-3}$. In Fig. 9b we zoom into the breather and show its portrait at a different times. The time corresponding to the left-most figure is $t = 0.0466$, and the time difference between every two neighboring figures is fixed to be $\Delta t = 1.865 \times 10^{-3}$. For clarity the different shapes the breather assumes, are displayed along the x-axis.

In Fig. 10, we display a more complicated breather that emerges from a 5-humps purely travelling compacton generated by (17), with $p = 5$ and $\delta =$

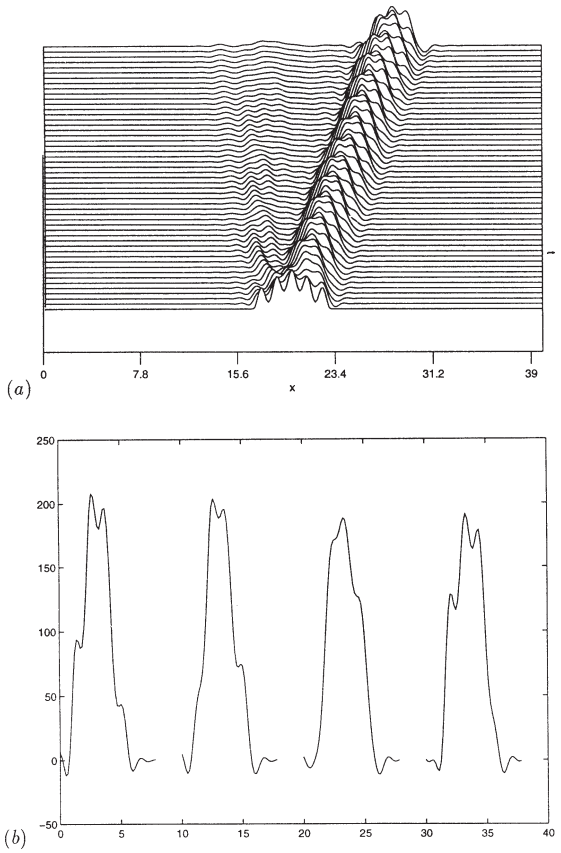

Fig. 10. A 4-humps breather evolving out of a 5-humps initial data, $p = 5$ in (17) ($\delta = (5/26)^2$). (a) Temporal evolution. (b) A separate snap-shot of the 4-humps breather in different times.

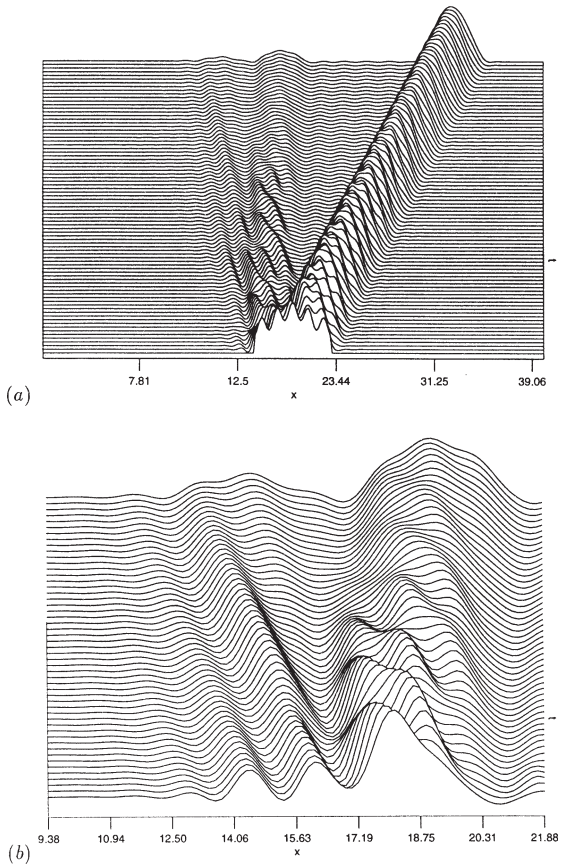

Fig. 11. Several breathers evolving out of a 5-humps initial data (25) ($\delta = (5/26)^2$). (a) Temporal evolution. (b) Zooming into the left side. At least one 3-humps breather emerges from the tail of the leading 4-humps compacton.

$(5/26)^2$, used as an initial data. As in the cubic case, this structure does not seem to be evolutionary. Its main part transforms into a stable 4-humps breather that propagates with a constant velocity. The time spacing between the different snap-shots is the same as in Fig. 9. The left plot in Fig. 10b describes the solution at $t = 0.0746$. The numerics was not sufficiently detailed to identify unambiguously the nature of the emerging shape on the left side of part (a) of the picture.

In the last displayed example we use the same initial domain, the same $\delta = (5/26)^2$, and the same homogeneous solutions but we reduce their relative components,

$$u_0(x) = 100[1 + \tfrac{1}{4}(\cos(x\sqrt{26}) + \cos(x\sqrt{26}/5))], \tag{25}$$

and zero elsewhere. As in the previous example, a 4-humps breather emerges on the right side of the pattern, but this time it leaves behind at least one 3-humps small breather, see Fig. 11. Possibly, a third multi-humps structure emerges, but the numerical resolution is not sufficient to make a definite statement. Fig. 11a corresponds to time $t \in [0, 0.149]$. In Fig. 11b we follow the evolution of the small, 3-humps breather for $t \in [0.056, 0.149]$. Note that in both breathers the humps decrease in time, and the 4-hump breather appears to transform into a single hump compacton. Here, as well, it is unclear whether that is a genuine phenomena or an artifact induced by the numerical methods in hand.

4. Comments and interim conclusions

(1) We have carried a large number of numerical simulations, of which a small sample was shown in the last section. These experiments seem to indicate that only one hump compactons propagate as a purely travelling wave. We find multi-humps structures that propagate with a constant speed, but these are breathers. Apart of the compact support their other features are quite similar to those observed in conventional breathers. However, one should keep in mind that, given the enormous variety of possible travelling structures, some of the presented conclusions may have a limited validity. Among the many interesting topics left for further exploration we mention the need to understand what causes the formation of a breather.

(2) In a recent work [8], Dey seeks for solutions of the form $A\cos^{\sigma}(Bs)$ for Eq. (3). Such solutions were found for $\sigma = 4/(m-1)$ and a specific value of δ. This solution is an exact counterpart of our 2-compacton (13) found for $\delta = 0.16$. Clearly, other P-compactons are unavailable via such an Ansatz. Dey also considers another nonlinearly dispersive quintic equation, derivable from a Lagrange principle, cf. Ref. [3], and, again, finds the same compacton solution for a specific numerical value of the quintic coefficient. A similar conclusion emerges from a recent work [9] where, in addition, the stability and evolutionarity of these compactons is numerically tested. Like their cubic siblings, these compactons are very robust.

(3) Perhaps the simplest way to see the origin for the richness of patterns generated by the quintic equation, as compared with the relative simplicity of the patterns in the cubic case, is to compare the dynamics of one oscillator with the large variety of modes generated by two coupled oscillators.

(4) The comparison with other efforts to understand quintic dispersive effects whether linear or not, makes the advantage of our model equation plainly clear; it is about *the only model which enables an analytical glimpse into the interaction of waves*. In particular, it helps us to understand how quintic dispersion generates a plethora of patterns not observed in the cubic case. While the particular form used in this work was not yet derived from any concrete problem, there is ample evidence to suggest that other quadratic dispersions, say the ones used in Ref. [9], produce very similar patterns. We believe that the understanding gained via the present problem will be useful in more concrete issues.

Appendix A

(1) The simplification used for Eq. (5) is also available for the fully nonlinear Boussinesq equations [2,10],

$$u_{tt} = u_{xx} - (u^{m+1})_{xx} - \delta[u(u^m)_{2x}]_{xx}\,, \quad m = 1, 2\,, \tag{A.1}$$

or

$$u_{tt} = (u^3)_{xx} + \delta[u(u^2)_{xx}]_{xx}\,. \tag{A.2}$$

A dissipative counterpart of our problem is given via

$$u_t + (u^2)_x + (uu_x)_x + \delta(uu_{3x})_x = 0\,. \tag{A.3}$$

Eq. (A.2) describes vibrations of a purely anharmonic lattice with a quartic potential, and in addition to a compact travelling waves it also admits a stationary compact breather [2]. Eq. (A.3) can be viewed either as a nonlinear variant of the KS equation or as the Hale–Shaw problem appended with a convection [11].

(2) We note that the amplitude-independent width of the trigonometric compactons is a result of detailed balance between convection and the dispersion, manifested in Eqs. (1), (5) and (A.1) via the same degree of homogeneity of the nonlinear mechanisms. If additional temporal derivatives are involved, this balance is lost and the resulting compactons always have a varying width. For instance, both for

$$u_{tt} = u_{xx} + (u^{m+1})_{xx} + \delta^2[u(u^n)_{xt}]_{xt}\,, \tag{A.4}$$

and

$$u_t + (u^{m+1})_x + b[u(u^n)_{tx}]_x + \delta[u(u^l)_{txxx}]_x = 0\,, \tag{A.5}$$

the presence of temporal derivatives has a dramatic impact on the resulting patterns. In both cases, if one fixes δ, changes in the speed of the wave generate a whole manifold of compact structures.

Acknowledgement

We would like to thank I. Matkov and G. Raphael for their help with Figs. 1–4. P.R. would also like to thank P. Olver and J.M. Hyman, and D.L. thanks C.-W. Shu for useful discussions. P.R. was supported in part by the BSF Grant 94-00283. The research of D.L. was supported in part by the applied mathematical sciences subprogram of the office of energy research, US Department of energy, under contract no. DE-AC03-76SF00098. Part of this work was done while D.L. was staying in ENS, Paris, supported by the European TMR Grant # ERBFMRXCT960033.

References

[1] P. Rosenau, J.M. Hyman, Phys. Rev. Lett. 70 (1993) 564.
[2] P. Rosenau, Phys. Rev. Lett. 73 (1994) 1737.
[3] P. Rosenau, Phys. Lett. A 211 (1996) 265.
[4] P. Rosenau, Phys. Lett. A 230 (1997) 305.
[5] P. Olver, P. Rosenau, Phys. Rev. E 53 (1996) 1900.
[6] S. Kichenassamy, P.J. Olver, SIAM J. Math. Anal 23 (1992) 1141.
[7] J.M. Hyman, P. Rosenau, Physica D 123 (1998) 502.
[8] B. Dey, Phys. Rev. E 57 (1998) 4734.
[9] F. Cooper, J.M. Hyman, A. Khare, Compacton solutions in a class of generalized fifth order KdV equations, preprint.
[10] P. Rosenau, to be published.
[11] P. Rosenau, A. Oron, to be published.